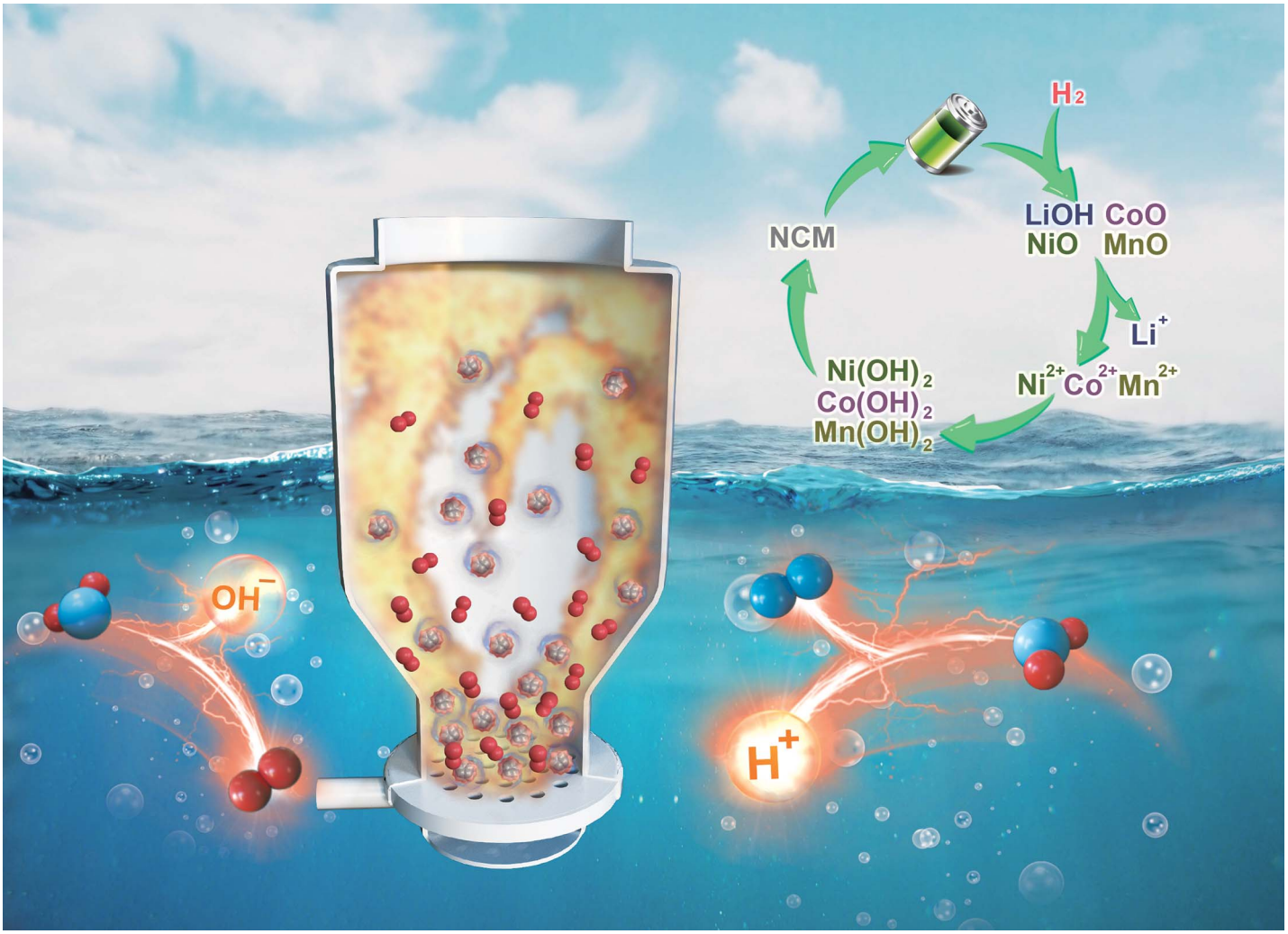

Showcasing research from Professor Xiaofei Guan's laboratory, School of Physical Science and Technology, ShanghaiTech University, Shanghai, China.

The critical role of H_2 reduction roasting for enhancing the recycling of spent Li-ion battery cathodes in the subsequent neutral water electrolysis

In this work, Ms. Jiayin Zhou (PhD candidate), Mr. Jihong Ni, and Prof. Xiaofei Guan developed a novel process that combines "H_2 metallurgy" and "water electrolysis" for recovering the valuable metal elements from the spent Li-ion battery cathodes. The water electrolysis not only creates a pH gradient for leaching and precipitating the transition metals, but also produces H_2 that is utilized to replace the H_2O_2 for reducing the cathode materials. This process holds great potential for industrial-scale recycling of spent Li-ion batteries in an effective and environmentally friendly way.

As featured in:

See Xiaofei Guan *et al.*, *RSC. Sustainability.*, 2023, **1**, 2241.

ROYAL SOCIETY OF CHEMISTRY

rsc.li/rscsus

Registered charity number: 207890

RSC Sustainability

ROYAL SOCIETY OF CHEMISTRY

PAPER

View Article Online
View Journal | View Issue

Cite this: *RSC Sustainability*, 2023, **1**, 2241

The critical role of H_2 reduction roasting for enhancing the recycling of spent Li-ion battery cathodes in the subsequent neutral water electrolysis†

Jiayin Zhou, Jihong Ni and Xiaofei Guan *

Effective and sustainable recycling of lithium-ion batteries is critically important for comprehensive resource utilization and environmental protection. Herein, we propose a novel recycling process that combines H_2 reduction roasting and neutral water electrolysis to recover valuable metal elements from the waste cathodes of spent lithium-ion batteries. Firstly, the waste cathode materials were calcined in H_2 to form oxides with lower valence transition metal ions. Then, the low-valence transition metal ions were leached from the reduced materials in the low-pH chamber and precipitated as hydroxides in the high-pH chamber of the neutral water electrolyzer. Three common LIB cathodes (*i.e.*, $LiCoO_2$, $LiMn_2O_4$, $LiNi_{0.5}Co_{0.2}Mn_{0.3}O_2$) were processed with this new combined method, and the leaching efficiencies of the Li ion and the transition metal ions significantly improved *versus* not using the reductive H_2 roasting. The leaching kinetics of $LiCoO_2$, $LiMn_2O_4$, $LiNi_{0.5}Co_{0.2}Mn_{0.3}O_2$, CoO, MnO, and NiO were carefully analyzed and compared to further understand the advantages of the combined method. The kinetics study supports the experimental finding that the transition metal elements are more easily leached from the roasted products than from the pristine cathode materials. Moreover, the H_2 produced at the cathode chamber of the neutral water electrolyzer can be recycled to the first step of reduction roasting, realizing the closed-loop utilization of H_2. This work highlights the critical role of H_2 reduction roasting in improving the recycling of the waste cathodes in the subsequent neutral water electrolysis.

Received 19th June 2023
Accepted 26th September 2023

DOI: 10.1039/d3su00201b

rsc.li/rscsus

Sustainability spotlight

The recycling of Li-ion batteries is becoming a matter of growing urgency because of the skyrocketing demand for new Li-ion batteries and the accumulation of enormous quantities of spent ones. The lack of feasible and sustainable recycling technologies will not only cause wastage of resources and environmental pollution, but also subdue the further penetration of Li-ion batteries in electric vehicles and grid-scale energy storage applications. Here, we develop a novel and effective solution that combines H_2 reduction roasting and neutral water electrolysis to recover valuable metals from the waste cathodes of spent Li-ion batteries. This work makes contributions to enable the UN Sustainable Development Goals 9 (industry, innovation and infrastructure), 12 (responsible consumption and production), and 13 (climate action).

1. Introduction

Lithium-ion batteries (LIBs) have become an indispensable part of the modern society since their commercialization. They have wide applications ranging from electric and hybrid vehicles, portable electronic devices, to stationary energy storage systems.[1–3] The rapid growth of the LIB market will lead to the accumulation of enormous amounts of spent LIBs. By the year 2035, 6.76 million spent LIBs will be generated per year.[4] Nevertheless, the percentage of LIBs recycled worldwide is still relatively low.[5,6] This gap motivates the research and development of novel technologies for recycling spent LIBs, which will not only alleviate the possible resource shortage in the future but also bring the benefits of economic growth and environmental protection.[7,8]

At present, there are four major methods to recover valuable metals from waste LIB cathode materials: hydrometallurgy, biometallurgy, pyrometallurgy, and direct recycling process. Among them, hydrometallurgical processes have received significant research attention because they consume less energy and enable a more efficient and comprehensive recovery of the valuable elements. Reducing agents are often used along with the acid leachant to lower the valence state of the transition metals (*e.g.*, Co, Mn) to +2 and thereby improve the leaching efficiency.[9,10] However, the conventional hydrometallurgical

School of Physical Science and Technology, ShanghaiTech University, Shanghai 201210, China. E-mail: guanxf@shanghaitech.edu.cn

† Electronic supplementary information (ESI) available. See DOI: https://doi.org/10.1039/d3su00201b

processes with convoluted chemistry often involve large consumption of chemicals, leading to the issues of high cost, waste generation and environmental pollution.[11]

Recently, the electrochemical pH gradient produced by neutral water electrolysis in an H-shaped electrolysis cell (H-cell) has been systematically investigated as an environmentally benign method to recover valuable metals from waste LIB cathodes (*e.g.*, $LiCoO_2$ (ref. 12) and $LiMn_2O_4$ (ref. 13)) in addition to decarbonating $CaCO_3$ (ref. 14 and 15) and direct air capture of CO_2.[16] This method shows promise in reducing the chemical consumption and simplifying the process. However, it is incompatible with the use of water-soluble reducing agents (*e.g.*, H_2O_2, $NaHSO_3$, $Na_2S_2O_5$, ethanol, or glucose)[4,12] in the anode chamber, because a portion of the reducing agent added would be inevitably consumed through oxidization at the anode. When not adding any external reducing agents, only the oxygen ions in the lattice of waste cathodes would serve as the reducing agent,[17] and the leaching kinetics would be slow. To circumvent the abovementioned issues and improve the leaching efficiencies of transition metals in the anode chamber of the neutral water electrolyser, the waste cathode materials of LIBs can be pretreated by reduction roasting. The previous studies on other different methods of recycling LIBs have reported various solid reductants for reduction roasting, such as graphite,[18–21] coal (*e.g.*, lignite),[22] and Al foil.[23] Although satisfactory leaching efficiencies in the subsequent water leaching are obtained, these solid reductants resulted in low product purity and required further treatment steps to remove residual reducing agents.[24] Gaseous reductants including NH_3,[25] CH_4,[26] and H_2 (ref. 27 and 28) have also been explored, and the results were promising in reducing the waste LIB cathodes.

In this work, we, for the first time, propose a novel combined process of H_2 reduction roasting and neutral water electrolysis to enable the effective and sustainable recovery of cathode materials from spent LIBs (Fig. 1). Firstly, the cathode material is reduced into low-valence metal oxides (MO; M: Co, Mn, or Ni)

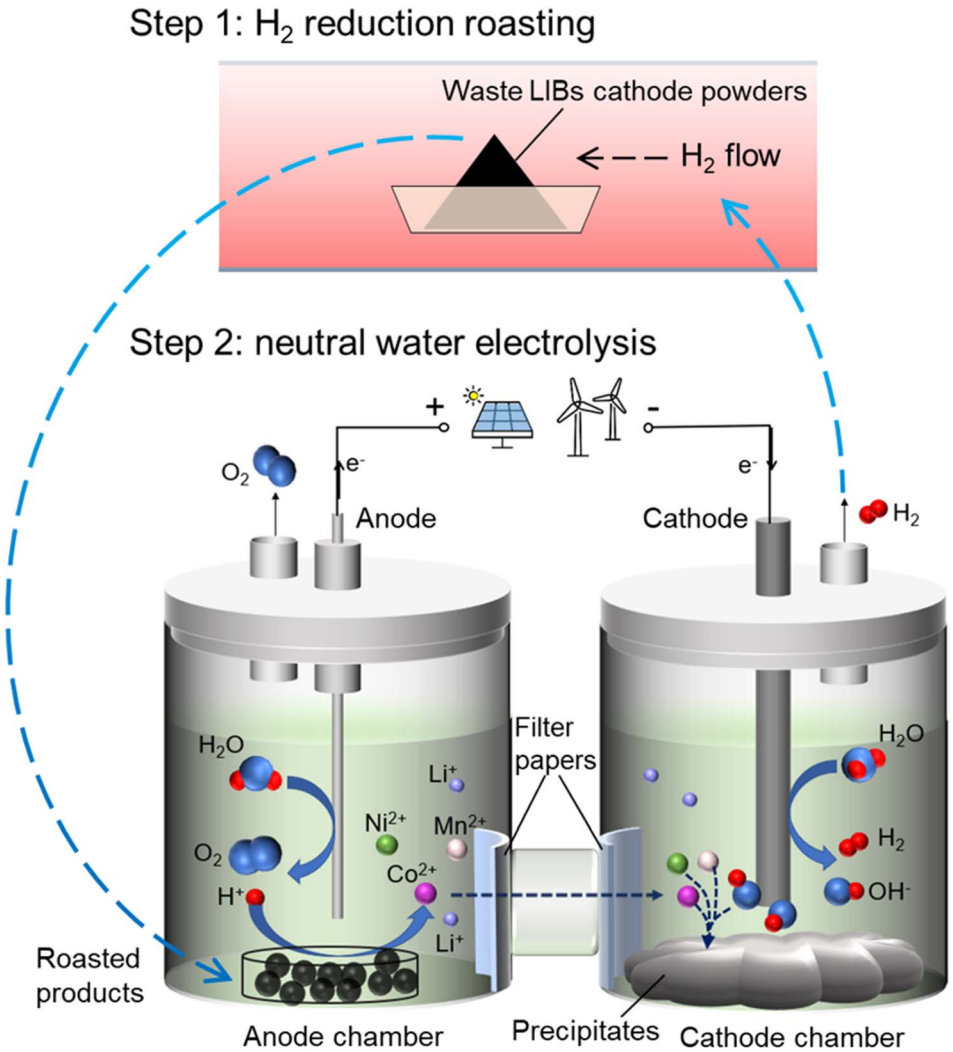

Fig. 1 Schematic of the combined method of H_2 reduction roasting and neutral water electrolysis. The waste LIB cathode powders contained in an alumina boat were first roasted in H_2 inside a furnace. Then, the roasted products were leached in the acidic anode chamber, and the transition metal ions were precipitated in the alkaline cathode chamber of the electrolyser. The H_2 produced from the hydrogen evolution reaction at the cathode chamber can be used as the gas reductant in the first step.

which are easy to dissolve in acid. The ideal chemical reactions between H_2 and $LiCoO_2$, $LiMn_2O_4$, or $LiNi_{0.5}Co_{0.2}Mn_{0.3}O_2$ are expressed by eqn (1)–(3). Then, the low-valence transition metal elements in the reduced cathode materials are efficiently leached and recovered using the pH gradient generated by neutral water electrolysis. During the neutral water electrolysis, the oxygen evolution reaction (OER, eqn (4)) occurs at the anode, which can provide H^+ for the dissolution of the reduced cathode materials, as described by eqn (5). The hydrogen evolution reduction (HER, eqn (6)) takes place at the cathode. The transition metal ions are transported from the anode chamber to the cathode chamber, where they are precipitated into hydroxides as represented by eqn (7). The mixed hydroxide precipitates can be readily separated from the electrolysis cell, after which the ratio of transition metals can be adjusted. The Li^+ that are leached out can be precipitated in the form of Li_2CO_3 (eqn (8)). The new layered ternary $LiNi_xCo_yMn_zO_2$ (NCM) can be synthesized from the Li_2CO_3 and the transition metal hydroxides recovered, closing the loop. In addition, some of the H_2 generated by water electrolysis can be recycled to the first step of reduction roasting. Compared with traditional hydrometallurgical methods, this new combined process minimizes the use of chemicals (*e.g.*, external acids, bases and reducing agents), generates no hazardous chemical waste, and also enables the closed-loop utilization of H_2. Therefore, this novel combined method is effective and environmentally friendly, and has industrial potential for large-scale recycling of spent LIBs.

$$2LiCoO_2 + H_2(g) = 2LiOH + 2CoO \quad (1)$$

$$2LiMn_2O_4 + 3H_2(g) = 2LiOH + 4MnO + 2H_2O(g) \quad (2)$$

$$LiNi_{0.5}Co_{0.2}Mn_{0.3}O_2 + 1/2H_2(g) = LiOH + 0.5NiO + 0.2CoO + 0.3MnO \quad (3)$$

$$H_2O = 1/2O_2 + 2H^+ + 2e^- \quad (4)$$

$$MO + 2H^+ = M^{2+} + H_2O\ (M^{2+}: Co^{2+}, Ni^{2+}, Mn^{2+}) \quad (5)$$

$$2H_2O + 2e^- = 2OH^- + H_2 \quad (6)$$

$$M^{2+} + 2OH^- = M(OH)_2\ (M^{2+}: Co^{2+}, Ni^{2+}, Mn^{2+}) \quad (7)$$

$$2Li^+ + CO_3^{2-} = Li_2CO_3 \quad (8)$$

2. Experimental

2.1. Pretreatment

The spent LIBs with the three common cathode chemistries ($LiCoO_2$, $LiMn_2O_4$, and $LiNi_{0.5}Co_{0.2}Mn_{0.3}O_2$) were purchased from recycling merchants located in Guangdong province, China. The recycling of LIBs with two other important cathode chemistries (*i.e.*, $LiFePO_4$, $LiNi_xCo_yAl_{1-x-y}O_2$) was not investigated in this work. The spent LIBs were fully discharged by immersing in a NaCl aqueous solution (1 mol L^{-1}) for 24 hours, and then manually disassembled inside a fume hood after washing and drying at room temperature. To remove the electrolyte and the binder, the cathode scraps consisting of Al foil and the cathode powders were transferred to a quartz-tube furnace and heated at 400 °C under vacuum for 5 hours.[29] Then, the cathode powders were easily peeled off. To decrease the particle size, the cathode powders were ground in a planetary ball mill at 500 rpm for two hours. The milling medium and the volume ratio used were consistent with the previous work.[12] Afterwards, DI water was added to the cathode powders to remove some graphite by flotation. Eventually, the cathode powders were dried and used in the electrolysis experiments. For convenience, these dried cathode powders were referred to as the pristine waste cathode powders. The composition was characterized by inductively coupled plasma optical emission spectroscopy (ICP-OES). For example, the molar ratio of Ni : Co : Mn was measured to be 5.02 : 2.1 : 2.88 in a batch of pristine waste ternary cathode materials. Considering the experimental error introduced in the process of sample solution preparation, the waste cathode material was inferred to be $LiNi_{0.5}Co_{0.2}Mn_{0.3}O_2$, hereinafter referred to as NCM523 (or NMC532).

2.2. H_2 reduction roasting

A certain quality of cathode material powders was added to an alumina boat, and reduction roasting was performed inside a quartz tube in an electric furnace. Ar gas was used to ensure an inert atmosphere during the heating process at 5 °C min^{-1}. When the furnace reached the target temperature, Ar was turned off and 5% H_2–95% Ar gas was flowed to the reactor at 150 mL min^{-1}. After the predetermined time elapsed, the 5% H_2–95% Ar was switched off and the roasted products were cooled to room temperature at 5 °C min^{-1} under Ar protection.

2.3. Electrochemical cells

The H-shaped electrochemical cells (H-cells) for water electrolysis were assembled following the process as described in Note S1.† Neutral water electrolysis experiments were carried out under different applied voltages, temperatures, durations, and solid-to-liquid ratios for recycling the waste cathode materials. The solid-to-liquid ratio is defined as the ratio of the mass of the pristine waste cathode powders to the volume of the aqueous electrolyte in the anode chamber (10 ml). Gamry™ Interface 1000 potentiostat (Gamry, PA, USA) was used for all electrochemical measurements. The pH values of the aqueous electrolyte in the anode and cathode chambers were measured by using a double-junction pH probe (Leici Instrument, Shanghai, China).

2.4. Regeneration of NCM523

A high-temperature solid-state reaction was used to resynthesize NCM523. In brief, the transition metal hydroxide precursor of the desired molar ratio (Ni : Co : Mn = 5 : 2 : 3) and the Li_2CO_3 powders recovered were mixed with a Li : (Ni + Co + Mn) molar ratio of 1.05 : 1 and ground with an agate mortar and pestle. The mixture was pressed into a pellet and then sintered at 950 °C for 10 h in air in a muffle furnace.

2.5. Materials characterization

The crystalline phases of the samples were characterized by using X-ray diffraction (XRD) with a Cu target and a θ–2θ geometry (Bruker™ D8). The XRD patterns were scanned with an increment of 0.02° and a scanning rate of 0.2° or 0.02° per second. The ICDD Powder Diffraction File (PDF)-4+ database was used for phase identification. Raman spectra (Andor Shamrock SR-500i) and the X-ray photoelectron spectroscopy (XPS; Thermo Fisher Scientific ESCALAB™ 250Xi) results of the samples were also collected. The surface morphologies and elemental distribution were observed using a scanning electron microscope equipped with an energy dispersive X-ray spectroscopy instrument (SEM-EDS, JEOL SEM IT-500HR).

Inductive coupled plasma optical emission spectroscopy (ICP-OES) was employed to determine the content of metal ions in the samples (Thermo Scientific ICP-OES iCAP™ 7400). The sample solution was prepared by first dissolving the sample in concentrated HCl (Sinopharm, 36.5%) and then diluting with DI water by 10 times. The leaching efficiencies of various metal ions from the powders were calculated from $\gamma_M = (c_M m - c'_M m')/c_M m$, where γ_M is the leaching efficiency of M (M: Li, Co, Ni and Mn); c_M and c'_M are the contents of M in the powders in the anode chamber before and after leaching, respectively; m and m' are the masses of the powders in the anode chamber before and after leaching, respectively.

2.6. Leaching kinetics analysis

Leaching of the commercially purchased high-purity oxide powders (CoO, MnO, NiO, $LiCoO_2$, $LiMn_2O_4$, and $LiNi_{0.5}Co_{0.2}Mn_{0.3}O_2$) was carried out in the standard sulfuric acid solutions (0.05 mol L^{-1}, 200 ml) in single-chamber glass reactors. The acid concentration was selected for two reasons: first, the pH value was stable during the leaching; second, the pH value was relatively low but close to the actual pH in the anode chamber during the neutral water electrolysis. In each experiment, the oxide powders (0.05 g) inside a removable quartz crucible were placed into the acid solution after reaching the desired temperature. The solution was then agitated with a magnetic stir bar at 450 rpm. During the leaching process, 1 ml of the solution was sampled at certain intervals to measure the leaching efficiency of each transition metal cation for the kinetics analysis.

The leaching process of the oxide powders in acid can be simplified into one of the three typical kinetic models: the liquid boundary layer mass transfer control model (eqn (9)), the surface chemical reaction control model (eqn (10)) and the residue layer diffusion control model (eqn (11)).[30] In these equations, X is the leaching efficiency of a metal cation, t is the reaction time (min); k_1, k_2 and k_3 are the specific reaction rate constants and also the slopes of the fitting lines for the three models, respectively.

$$X = k_1 t \tag{9}$$

$$1 - (1 - X)^{\frac{1}{3}} = k_2 t \tag{10}$$

$$1 - 3(1 - X)^{\frac{2}{3}} + 2(1 - X) = k_3 t \tag{11}$$

After obtaining the values of specific rate constant, k, at various temperatures, the data were fitted to the Arrhenius relationship as described by eqn (12),[31] where A is the pre-exponential factor (min^{-1}), R is the gas constant (8.31 J mol^{-1} K^{-1}), E_a is the apparent activation energy for the leaching of a certain type of metal cation (J mol^{-1}), and T is the absolute temperature (K). The value of E_a can be obtained as the slope of the ln k *vs.* $-1/RT$ curve. It is noted that the factor A varies with the experimental conditions including the acid concentration and the solid-to-liquid ratio.[32]

$$k = A\, e^{-\frac{E_a}{RT}} \tag{12}$$

3. Results and discussion

3.1. Recycling $LiCoO_2$

3.1.1. H_2 reduction roasting of $LiCoO_2$. The goal of H_2 roasting was to reduce the waste $LiCoO_2$ to low-valence CoO that was easily soluble in acid, as expressed by eqn (1). The effect of temperature was investigated by varying the temperature from 375 °C to 500 °C for 50 min. Fig. 2A shows the XRD patterns of the pristine waste $LiCoO_2$ and the roasted products that were calcined in 5% H_2 or Ar at different temperatures (375 and 500 °C). The diffraction peaks of the pristine waste cathode powders were indexed to be the $LiCoO_2$ phase. After the reduction in 5% H_2 at 375 °C for 50 min, the diffraction peaks for $LiCoO_2$ disappeared, and the CoO phase was observed. It's noted that no diffraction peaks for Li-containing product (*e.g.*, LiOH or Li_2CO_3) were observed likely because the amount was below the XRD detection limit or the phase crystallinity was poor. The ICP-OES results revealed 60.91 wt% of Co and 4.88 wt% of Li present in the 0.045 g roasted product, verifying the presence of Li element. When the temperature rose to 500 °C, the reduction product was mainly a mixture of CoO and Co. The formation of Co was owing to the relatively low thermodynamic stability of CoO against H_2 reduction (Fig. S1†). The Co metal was an undesired product because a higher temperature and higher H_2 consumption were required. Moreover, in the subsequent neutral water electrolysis step, the Co metal would react with H^+ to produce H_2 in the anode chamber where O_2 was also generated (Fig. 1), causing safety risks. Therefore, it was necessary to control the degree of reduction and avoid the production of the metal phase for energy saving and safety. We also performed a control experiment of calcining pristine $LiCoO_2$ in pure Ar at 375 °C for 50 min to evaluate the reducing capacity of residual carbon in the waste cathode material. As shown in Fig. 2A(b), strong diffraction peaks of $LiCoO_2$ remained and only a tiny amount of CoO was generated in the roasted product, indicating that the reducing capacity of carbon was negligibly small compared with that of 5% H_2 (Fig. 2A(c)). The formation of the minor phase of CoO was from the reaction between the $LiCoO_2$ and the residue carbon,[22] as expressed by $4LiCoO_2 + C = 4CoO + Li_2O + Li_2CO_3$. Based on the results in Fig. 2A, the product obtained by roasting the pristine $LiCoO_2$ at 375 °C for 50 minutes in 5% H_2 was used for the following step of neutral water

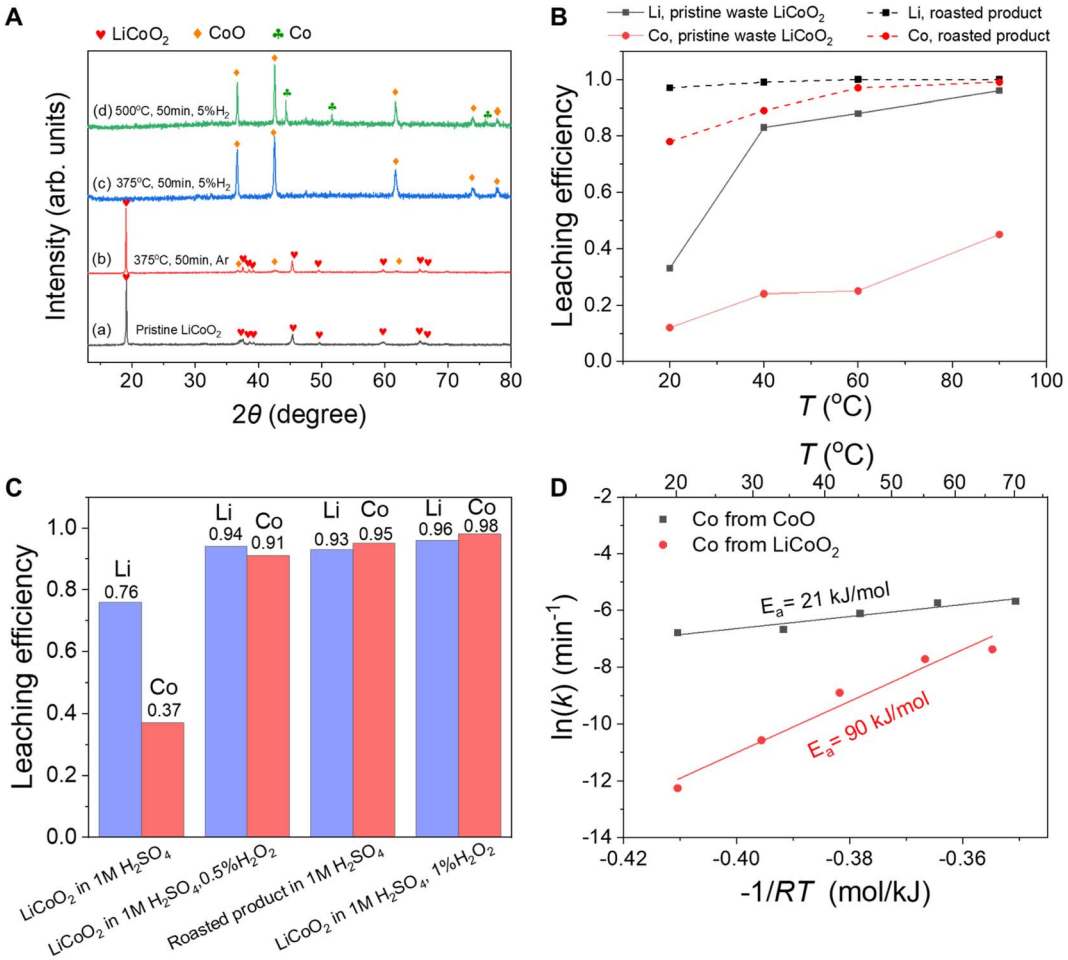

Fig. 2 (A) The XRD patterns of (a) the pristine waste $LiCoO_2$ and the roasted products obtained at (b) 375 °C for 50 min in Ar, (c) 375 °C for 50 min in 5% H_2, (d) 500 °C for 50 min in 5% H_2. The diffraction peaks were indexed to $LiCoO_2$ (PDF No. 01-075-3201), CoO (PDF No. 01-076-3830) and Co (PDF No. 00-001-1255). (B) The leaching efficiencies of Li and Co from the pristine waste $LiCoO_2$ and the roasted products in H-cells with an applied voltage of 3.5 V and a solid-to-liquid ratio of 10 g L^{-1} at different temperatures (20, 40, 60 and 90 °C) for 24 h. (C) The leaching efficiencies of Li and Co from pristine waste $LiCoO_2$ in 1 mol L^{-1} H_2SO_4 containing varying concentrations of H_2O_2 and from the roasted product in 1 M H_2SO_4 with no H_2O_2 at 40 °C for 30 min. (D) Kinetics analysis showing the Arrhenius plots for the Co leaching from the commercially purchased CoO and $LiCoO_2$ in 0.05 mol L^{-1} H_2SO_4 solution.

electrolysis. It's noted that the temperature conditions required here are relatively mild compared with the current pyrometallurgical options summarized in a recent comprehensive review.[33] In particular, Umicore's industrial-scale pyrometallurgical process typically operates at 1200–1450 °C in the smelting zone.[34] Therefore, the H_2 reduction roasting investigated here has the potential to lower the energy consumption for recycling the waste cathodes of LIBs.

The roasted product treated with 5% H_2 at 375 °C for 50 minutes was further characterized using XPS. Based on the core-level C 1s XPS spectrum (Fig. S2†), there were two kinds of carbon species on the surface of the roasted product. The major peak at ~284.8 eV was attributed to the adventitious carbon, while the other major peak at ~290 eV was assigned to the carbonate.[35] As shown in the core-level Co 2p XPS spectra (Fig. S3†), the binding energy of Co $2p_{3/2}$ in the pristine waste $LiCoO_2$ was ~780.1 eV, and the separation of the binding energies of Co $2p_{3/2}$ and Co $2p_{1/2}$ was ~15 eV. In comparison, the separation of the binding energy of Co $2p_{1/2}$ and Co $2p_{3/2}$ of the roasted product was ~15.8 eV, confirming the change of the Co valence state from +3 to +2 after the H_2 roasting.[12]

3.1.2. Neutral water electrolysis for treating the roasted product of $LiCoO_2$. The pristine waste $LiCoO_2$ and the roasted product were separately treated in the anode chambers of H-Cells. Fig. 2B shows the leaching efficiencies of Li and Co from the waste $LiCoO_2$ powders and the roasted products performed at 3.5 V for 24 h at different temperatures (20, 40, 60 and 90 °C) with a solid-to-liquid ratio of 10 g L^{-1}. It was easier to leach both Li^+ and Co^{2+} from the roasted product. The leaching efficiencies of Li and Co from the roasted products reached 100% and 97%, respectively, in the electrolysis experiment at 60 °C. In comparison, the leaching efficiencies of Li and Co from the pristine $LiCoO_2$ were only 88% and 25%, respectively, under the same electrolysis conditions. The difference indicated that the combined process of H_2 reduction and neutral water electrolysis was a feasible approach in increasing the

leaching efficiencies of Li and Co. The H_2 gas served as an effective reducing agent in a reductive roasting pretreatment and promoted the leaching of Co^{2+} during the neutral water electrolysis. After 24 hours of electrolysis at 90 °C, Co^{2+} was recovered in the form of $Co(OH)_2$. Among them, part of the Co^{2+} was directly precipitated in the alkaline cathode chamber and separated by filtering, and the remaining was precipitated by mixing the anolyte and the catholyte and then adjusting the pH to approximately 11. The total recovery rate of Co^{2+} reached nearly 100%, similar to a previous report.[12] It's worth mentioning that, to minimize the operation steps, there might be no need to directly mix the anolyte and the catholyte in practice; as the $Co(OH)_2$ precipitates in the cathode chamber are separated by filtering, the remaining Co^{2+} would be continuously transported by diffusion and convection from the low-pH anode chamber through the cross-tube to the high-pH cathode chamber for precipitation. It's also noted that, due to the presence of LiOH in the roasted product (eqn (1)), the total electrolyte solution was alkaline after performing the electrolysis and separating the precipitates. However, the solution can be adjusted to neutral pH by adding sulfuric acid and reused as the electrolyte for new leaching cycles.

3.1.3. Comparison of the reduction effects of H_2 and H_2O_2. Experiments were performed to compare the effects of the H_2 reduction roasting and the direct addition of H_2O_2 to H_2SO_4 solution for leaching $LiCoO_2$. The roasted product was treated in H_2SO_4 solutions (1 M) with no H_2O_2. Pristine waste $LiCoO_2$ powders (0.5 g) were treated in H_2SO_4 solutions (1 mol L^{-1}, 1 M) containing varying concentrations of H_2O_2 (0, 0.5%, and 1%). The experiments were all performed at 40 °C for 30 min. The temperature of 40 °C was selected based on the trade-offs between the greater decomposition rate of H_2O_2 at higher temperatures and the slower leaching kinetics at lower temperatures. The reaction time of 30 min was chosen to manifest the significant differences because an excessively long time would result in nearly complete leaching while a much shorter time might cause too little leaching in all the tests.

As shown in Fig. 2C, the leaching efficiencies of Li and Co of pristine waste $LiCoO_2$ in 1 M H_2SO_4 without H_2O_2 were 0.76 and 0.37, respectively. When the roasted product directly reacted with 1 M H_2SO_4, the leaching efficiencies of Li and Co reached as high as 0.93 and 0.95, respectively. The results were comparable to the leaching efficiencies of $LiCoO_2$ in 1 M H_2SO_4 containing 0.5% H_2O_2 or 1% H_2O_2. In other words, the reduction effect of H_2 roasting pretreatment was comparable to that of adding 0.5–1% H_2O_2 to acid. As an environmentally benign reducing agent, H_2O_2 is widely adopted as a reducing agent in scientific research and industrial processes; however, it is relatively expensive and decomposes readily upon exposure to light or heat, leading to cost increase and waste of resources.[4] In comparison, the use of H_2 reduction roasting might be more advantageous especially considering that the excess H_2 can be recirculated.

3.1.4 Kinetics analysis for the Co leaching from CoO and $LiCoO_2$. The leaching kinetics analysis was performed to further understand the difference in the Co leaching from CoO and $LiCoO_2$. We explored the leaching behaviors of Co from the commercially purchased CoO and $LiCoO_2$ in 0.05 mol L^{-1} H_2SO_4 for different time lengths (0–60 min) at various temperatures (20–70 °C), as shown in Fig. S4a and S5a.† The leaching kinetics of Co from CoO fit well with the surface chemical reaction control model (Fig. S4c†), while the leaching kinetics of Co from $LiCoO_2$ fit well with the residue layer diffusion control model (Fig. S5d†). This was because, unlike the leaching of Co^{2+} from CoO, the high valence Co^{3+} in the $LiCoO_2$ could not be readily leached into the solution without the use of an effective reductant (*e.g.*, H_2O_2), resulting in the formation of a residue layer and limiting the mass transfer. The values of the specific rate constant (k) obtained were used to plot the Arrhenius relationships, as shown in Fig. 2D. The activation energy values (E_a) were determined to be 21 kJ mol^{-1} and 90 kJ mol^{-1} for the Co leaching from CoO and $LiCoO_2$, respectively. The difference between the values of E_a was consistent with the experimental finding that the Co element was more easily leached from CoO than from $LiCoO_2$. The water soluble Co^{2+} can be directly leached out from CoO, while the leaching of $LiCoO_2$ involves the conversion from Co^{3+} to Co^{2+} first.[36,37]

3.2 Recycling $LiMn_2O_4$

3.2.1. H_2 reduction roasting of $LiMn_2O_4$. The roasting behaviors of the pristine waste $LiMn_2O_4$ in H_2 and Ar atmospheres were studied at different temperatures for 2 hours. Fig. 3A shows the XRD patterns of the pristine waste $LiMn_2O_4$ and the roasted products. After the reduction in 5% H_2 at 400 °C (Fig. 3A(b)), the diffraction peaks of $LiMn_2O_4$ disappeared, and the peaks of MnO and a mixture of orthogonal and monoclinic $LiMnO_2$ were observed. However, $LiMnO_2$ was not the desired product due to the presence of the Jahn–Teller active Mn^{3+} ions,[38] which, in contact with acid, would disproportionate to the easily soluble Mn^{2+} ions and the stable Mn^{4+} ions in the lattice.[39] When the pristine $LiMn_2O_4$ was roasted at 850 °C in an Ar atmosphere, the $LiMn_2O_4$ was transformed into Mn_3O_4 and orthogonal $LiMnO_2$ as the dominant phases and MnO as a minor phase. In contrast, the $LiMn_2O_4$ was completely transformed into MnO in 5% H_2 atmosphere at 850 °C (Fig. 3A(d)), as expressed by eqn (2). No metallic Mn phase was observed owing to the high thermodynamic stability of MnO against H_2 reduction (Fig. S1†). It's also noted that the signals of Li-containing species (*e.g.*, LiOH or Li_2CO_3) were below the XRD detection limit. Nevertheless, the ICP-OES results revealed 71.05 wt% of Mn and 2.55 wt% of Li in the roasted product (0.049 g) treated with 5% H_2, confirming the presence of the Li element. Fig. S6† shows the core-level Mn 3s XPS spectra of the pristine waste $LiMn_2O_4$ and the roasted product treated with 5% H_2 at 850 °C for 2 hours. The Mn 3s spectrum exhibited two split components due to the parallel spin coupling of the 3s electron with the 3d electron.[13,40] The magnitude of the peak splitting (ΔBE) of Mn 3s was 5.04 eV for the pristine waste $LiMn_2O_4$. Based on the approximate linear relationship between ΔBE and the Mn valence,[41] the average valence of Mn in the pristine waste $LiMn_2O_4$ was estimated to be approximately 3.5. In comparison, the magnitude of the peak splitting of Mn 3s was 5.82 eV for the roasted product, suggesting the valence of Mn

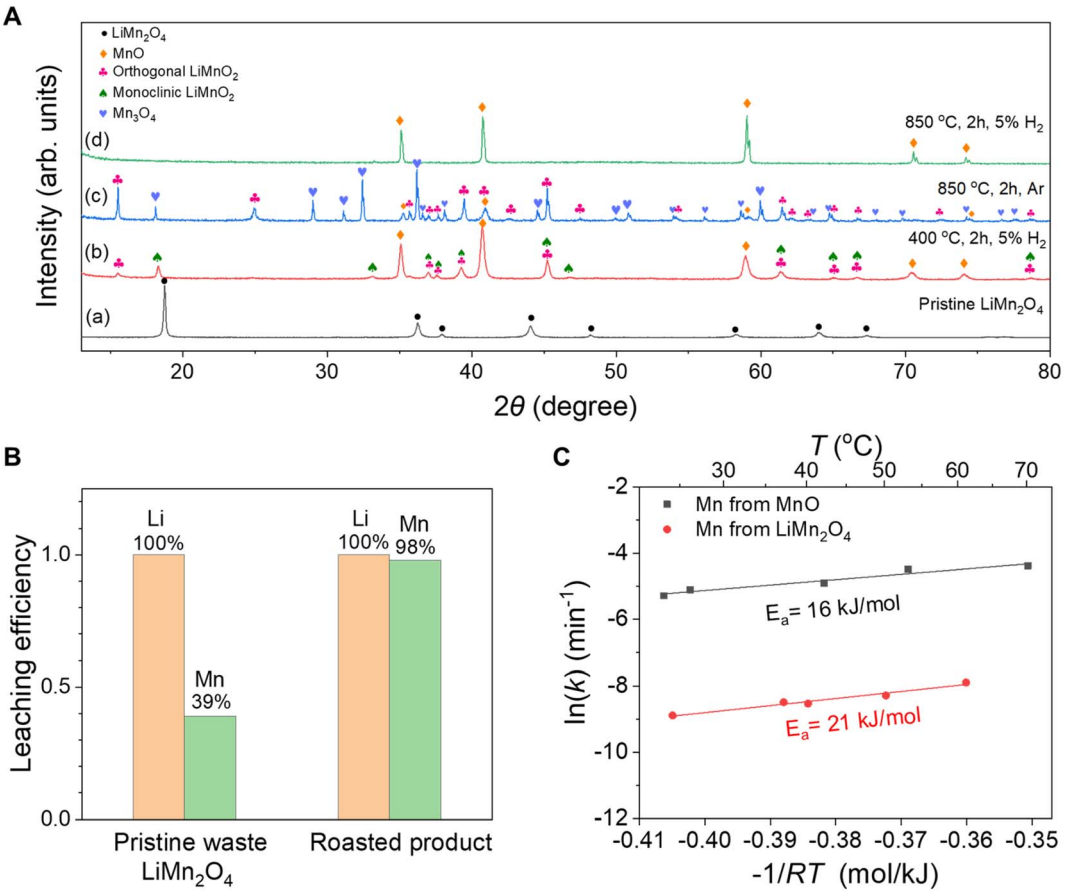

Fig. 3 (A) XRD patterns of (a) the pristine waste $LiMn_2O_4$ and the roasted products treated (b) in 5% H_2 at 400 °C, (c) in Ar at 850 °C, and (d) in 5% H_2 at 850 °C for 2 hours. The diffraction peaks were indexed to $LiMn_2O_4$ (PDF No. 04-008-6541), MnO (PDF No. 00-003-1145), orthogonal $LiMnO_2$ (PDF No. 00-035-0749), monoclinic $LiMnO_2$ (PDF No. 00-052-1347), and Mn_3O_4 (PDF No. 01-075-1560). (B) The leaching efficiencies of Li and Mn from the pristine waste $LiMn_2O_4$ and the roasted product (treated in 5% H_2 at 850 °C for 2 h) after neutral water electrolysis at 3.5 V for 24 h at 90 °C with a solid-to-liquid ratio of 10 g L^{-1}. (C) Kinetics analysis showing the Arrhenius plots for the Mn leaching from the commercially purchased MnO and $LiMn_2O_4$ in 0.05 mol L^{-1} H_2SO_4 solution.

close to 2. The Mn 3s XPS result of the roasted product confirmed the formation of MnO by H_2 reduction of the pristine waste $LiMn_2O_4$, consistent with the XRD results (Fig. 3A(d)). Based on the XRD and XPS results, the roasted product treated with 5% H_2 at 850 °C for 2 h was used for the following step of neutral water electrolysis.

3.2.2. Neutral water electrolysis for treating the roasted product of $LiMn_2O_4$. The pristine waste $LiMn_2O_4$ and the roasted product were treated in the anode chambers of different H-cells. Each experiment was performed at 3.5 V and a solid-to-liquid ratio of 10 g L^{-1} for 24 h at 90 °C. The leaching efficiencies of Li and Mn from the pristine waste $LiMn_2O_4$ were 100% and 39%, respectively (Fig. 3B). When the spinel $LiMn_2O_4$ reacted with the acid in the anode chamber, the Li^+ easily leached out from the tetrahedral sites of the structure. The Jahn–Teller active Mn^{3+} ions in $LiMn_2O_4$ disproportionated to Mn^{2+} ions and Mn^{4+} ions, of which the Mn^{2+} ions easily dissolved into the acid while the Mn^{4+} ions were more prone to stay in the lattice.[39] More detailed discussion on the leaching behavior of the pristine waste $LiMn_2O_4$ is provided in a previous report.[13] The leaching efficiencies of Li and Mn from the roasted product reached 100% and 98%, respectively (Fig. 3B). The significant improvement in the leaching efficiency of Mn was attributed to the H_2 reduction roasting step that reduced the oxidation state of Mn to +2.

3.2.3. Kinetics analysis for the Mn leaching from MnO and $LiMn_2O_4$. To gain further insights, the leaching kinetics analyses for the Mn leaching were performed. Fig. S7a and S8a† present the leaching efficiencies of Mn from the commercially purchased MnO and $LiMn_2O_4$ in 0.05mol L^{-1} H_2SO_4 solutions for different time lengths (0–60 min) at various temperatures (23–70 °C). Based on the curve fitting results, the leaching kinetics of Mn from MnO was controlled by the surface chemical reaction (Fig. S7c†), similar to the leaching of Co from CoO, whereas the leaching kinetics of Mn from $LiMn_2O_4$ was controlled by the residue layer diffusion (Fig. S8d†), similar to the leaching of Co from $LiCoO_2$. Using the Arrhenius relationship between ln k and $-1/RT$, the activation energies for the Mn leaching from MnO and $LiMn_2O_4$ were determined to be 16 kJ mol^{-1} and 21 kJ mol^{-1}, respectively (Fig. 3C). For $LiMn_2O_4$, the dissolution of Mn was initially facilitated by the Jahn–Teller effect;[37,39] however, further leaching of the Mn was limited by

the highly covalent Mn(IV)–O bonds.[13,39] In comparison, for the Mn leaching from MnO, the value of E_a was slightly smaller and the value of ln(k) was larger, confirming that the MnO was more easily soluble in acid than $LiMn_2O_4$.

3.3. Recycling NCM523

3.3.1. Neutral water electrolysis for treating the pristine waste NCM523. Although NCM has a similar layered structure and chemical properties to $LiCoO_2$, the recycling of NCM using the electrochemical pH gradient method is expected to be more complicated due to the existence of multiple transition metals in NCM. In addition, the experimental studies on the exact roles of multiple variables in the leaching of NCM as well as the associated phase evolution during the neutral water electrolysis have not been reported in the literature. Therefore, we first designed and performed a series of neutral water electrolysis experiments with pristine waste NCM powders that were not pretreated with H_2. Several parameters including temperature, applied voltage, duration and solid-to-liquid ratio were investigated to obtain the optimum leaching efficiency of Li, Ni, Co and Mn from waste NCM523 powders.

Fig. 4A shows the leaching efficiencies of Li, Ni, Co and Mn from waste NCM523 powders at different temperatures (25, 40, 60, 80, and 90 °C). In this series of experiments, the solid-to-liquid ratio was 10 g L^{-1}, the voltage was 3.5 V, and the leaching time was 24 hours. The leaching efficiency of the four metal elements all increased with temperature. This was mainly because the temperature increase caused the electrolyte ohmic resistance to decrease, and sped up the kinetics of the leaching reaction, resulting in a higher concentration of H^+ in the anode chamber. The leaching behavior of Li in NCM523 was similar to that in $LiCoO_2$ reported in a previous study.[12] The leaching efficiency of Li increased from 47% to 82.3% as the temperature increased from 25 °C to 40 °C and gradually increased to 89% at 90 °C. The leaching behavior of Ni and Co increased rapidly from 20.2% and 19.2% at 25 °C to 52% and 41.5% at 40 °C, and

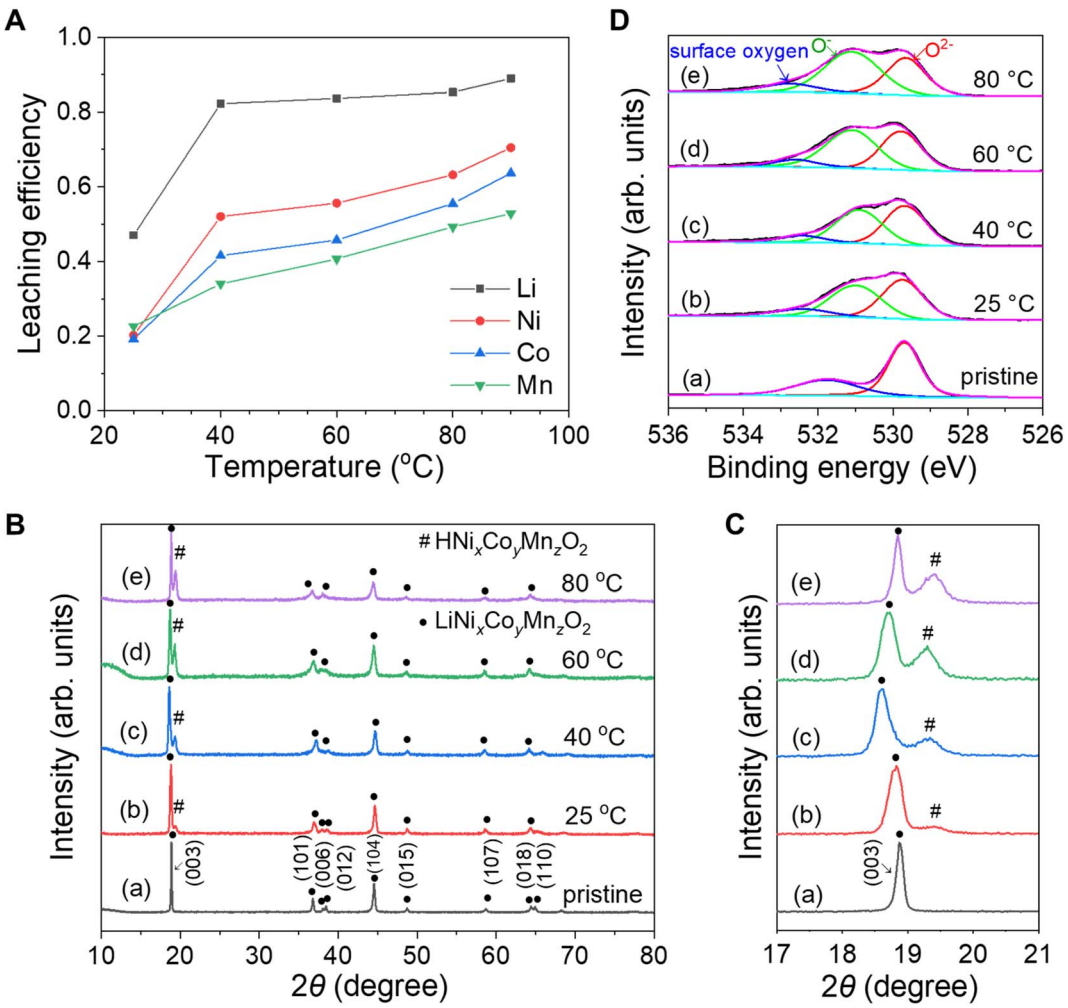

Fig. 4 (A) The leaching efficiencies of Li, Ni, Co, and Mn from the waste NCM523 powders performed at different temperatures (25, 40, 60, 80, and 90 °C) with an electrolysis voltage of 3.5 V and a solid-to-liquid ratio of 10 g L^{-1} for 24 hours. (B) The XRD patterns, (C) the magnified XRD patterns in the $2\theta = 17–21°$ range, and (D) the high-resolution O 1s XPS spectra of (a) the pristine waste powders and the residue powders after leaching at (b) 25 °C, (c) 40 °C, (d) 60 °C and (e) 80 °C in the anode chambers of the H-cells. In (D), the fitting curve (purple) for each of the O 1s XPS spectra (black) consists of a set of components attributed to the background (cyan), the adsorbed oxygen surface species (blue), the O^- (green), and the O^{2-} (red).

then gradually increased to 70.5% and 63.7% at 90 °C, respectively. Although the bond dissociation energies of Ni–O and Co–O were close,[42] the leaching efficiency of Ni was slightly higher than that of Co, because a significant portion of the Ni in NCM523 was in the divalent state[43] and was relatively easy to leach without the reduction.[37] The leaching efficiency of Mn gradually increased with temperature, but reached only 52.8% at 90 °C. This was because the Mn(IV)–O bond was more stable than the Ni–O bond and the Co–O bond, rendering the leaching of Mn more difficult. The results were consistent with the previous reports that Mn played a role of stabilizing the structure of the ternary NCM materials.[44,45]

The residue powders after leaching at different temperatures were characterized by XRD. It is noted that the amount of residue powders after leaching at 90 °C was too little to characterize. Fig. 4B and C show the XRD patterns for the waste NCM523 powders before leaching and after leaching at different temperatures (25, 40, 60, and 80 °C) for 24 hours. The powders maintained the α-$NaFeO_2$ structure after leaching. The peak splitting of (006)/(012) and (018)/(110) was unclear and amalgamated into one peak, indicating a disordered lamellar phase, with a mixing of lithium and metal ions. The (003) diffraction peak implied that all the residue powders retained a layer structure in the *c*-axis direction. Compared with the XRD pattern of the pristine sample as shown in Fig. 4C(a), the (003) diffraction peak for the residual powders shifted toward lower 2θ, which was caused by the increased lattice parameters in the *c*-axis direction. Due to the decreasing lithium content, the electrostatic repulsion between the oxygen anions increased and the distance between the metal–oxygen octahedral layers increased. It was noted that the (003) diffraction peak shifted toward higher 2θ after leaching at 60 °C and 80 °C compared with that after leaching at 25 °C and 40 °C, likely due to the migration of Ni^{2+} to the Li^+ layer. Ni^{2+} (0.069 nm)[46] and Li^+ (0.076 nm)[47] have similar radii. Since Ni^{2+} has one more positive charge than Li^+, when the Ni^{2+} occupied the vacancies created by the removal of Li^+, the electrostatic attraction between Ni–O reduced the distance between metal–oxygen octahedral layers, resulting in the decrease of the lattice parameter in the *c*-axis direction,[48] so the (003) diffraction peak shifted toward higher 2θ. It's noted that the claim for Ni^{2+} might also be applicable to Co^{3+} (radius: 0.0545 nm)[49] in the lattice which has two more positive charges than Li^+. Another revealing finding of this study was the observation of a small diffraction peak next to the (003) diffraction peak at higher 2θ value in all patterns after leaching, indicating the ion exchange between H^+ and Li^+ during leaching.[12] With the increase of temperature, the intensity of this peak gradually increased, indicating that higher temperature accelerated the exchange of H^+ and Li^+, and promoted the formation of the $HNi_xCo_yMn_zO_2$ phase.

The residue powders after leaching at different temperatures were also characterized by XPS. The high-resolution XPS spectra of Co 2p, Ni 2p, Mn 2p and Mn 3s did not show obvious changes (Fig. S9†). The dramatic change of high-resolution XPS spectra of O 1s confirmed that lattice oxygen played a vital role during leaching (Fig. 4D).[12,17] The O 1s spectrum of the pristine waste NCM523 powders displayed two main peaks. A well-defined peak observed at 529.7 eV was characteristic of O^{2-} anions of the crystalline network, whereas the peak at 531.8 eV was attributed to the adsorbed oxygen surface species. Interestingly, a new peak attributed to O^- at 531 eV appeared after leaching and the intensity of this peak gradually increased with increased leaching efficiency. The O^-/O^{2-} intensity ratio increased from 0.81 at 25 °C to 0.86 at 40 °C, 1 at 60 °C and 1.11 at 80 °C (Table S1†), indicating that the electrons of lattice oxygen were transferred to transition metals during leaching.

In addition to temperature, other parameters on the leaching efficiency of Li, Ni, Co and Mn from waste NCM523 powders were also carefully investigated. The effect of applied voltage and duration is discussed in Note S2 and Fig. S10.† The effect of solid-to-liquid ratio is discussed in Note S3, Fig. S11 and S12 in the ESI.† The optimal leaching conditions were determined to be an electrolysis voltage of 3.5 V, a solid-to-liquid ratio of 10 g L^{-1}, and a temperature of 90 °C. Overall, the leaching rates of the metals from NCM523 were still relatively slow due to the lack of external reducing agents.

3.3.2. H_2 reduction roasting of NCM523. To improve the leaching efficiencies of metals, the pristine waste NCM523 powders were first roasted in H_2. The XRD patterns of the roasted products at different temperatures, durations, and atmospheres are presented in Fig. 5A. There was almost no change in the phase before and after the reduction at 300 °C for 40 minutes in 5% H_2 atmosphere (Fig. 5A(c)). When the reaction time was extended to 135 minutes, the diffraction peaks of NCM523 became much weaker, and the peaks of the desired low-valence metal oxides including NiO and CoO were observed (Fig. 5A(d)). No other Mn-containing oxides were identified likely because their signals were below the XRD detection limit. When performing the reduction at a higher temperature (500 °C) for 35 minutes, the diffraction peaks of the undesired phases (*e.g.*, Ni, Co, and $LiMnO_2$) emerged (Fig. 5A(e)). The corresponding reaction between H_2 and NCM523 can be expressed as $LiNi_{0.5}Co_{0.2}Mn_{0.3}O_2 + 1.05H_2(g) = 0.7LiOH + 0.5Ni + 0.2Co + 0.3LiMnO_2 + 0.7H_2O(g)$. We also performed a control experiment of calcining pristine NCM523 powders in pure Ar at 300 °C for 135 min to evaluate the reducing capacity of residual carbon in the waste cathode material. The roasted products still maintained the α-$NaFeO_2$-type structure (Fig. 5A(b)), indicating that the reduction effect of the residual carbon was negligible. Based on these results, the products obtained by roasting the pristine NCM523 powders at 300 °C for 135 minutes in 5% H_2 were used for the following step of neutral water electrolysis. Moreover, the SEM and EDS mapping results for the roasted products at 300 °C for 135 minutes in 5% H_2 were compared with those for the pristine waste NCM523 powders (Fig. S13†). The pristine waste NCM523 materials were agglomerated particles that were closely bound (Fig. S13a†). In comparison, the agglomeration of the roasted products was relatively loose, and the shape was less regular (Fig. S13f†). The representative EDS mapping for both materials displayed homogeneous distributions of Ni, Co, and Mn (Fig. S13b–e and S13g–j†).

3.3.3. Neutral water electrolysis for treating the roasted product of NCM523. During the neutral water electrolysis, the roasted products were placed in the anode chamber of the cell.

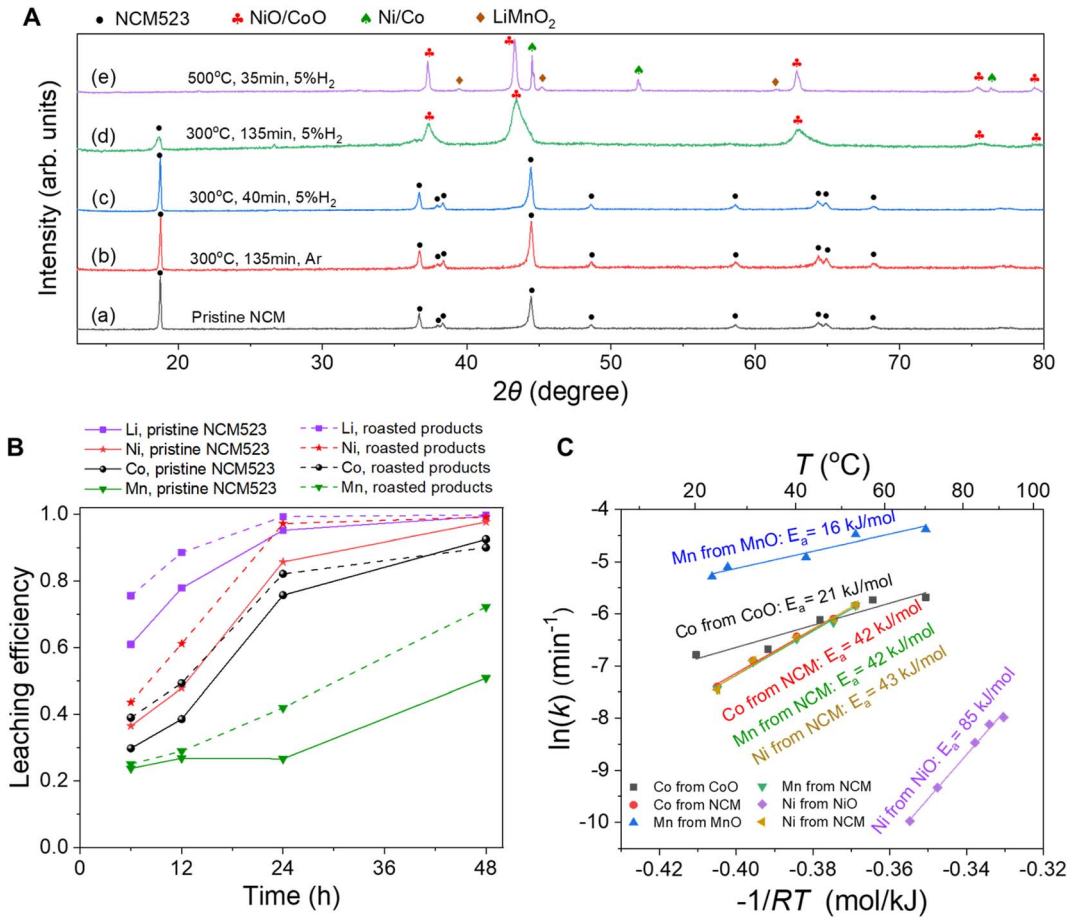

Fig. 5 (A) The XRD patterns of (a) the pristine waste NCM523 and the products roasted at (b) 300 °C for 135 min in Ar, (c) 300 °C for 40 min in 5% H_2, (d) 300 °C for 135 min in 5% H_2, (e) 500 °C for 35 min in 5% H_2. Scanning rate: 0.02° s^{-1}. The data from the reference on $LiNi_xCo_yMn_zO_2$ (ref. 16) and the standard cards of NiO (PDF No. 00-004-0835), Ni (PDF No. 00-001-1260), CoO (PDF No. 00-43-1004), Co (PDF No. 00-15-0806), and orthogonal $LiMnO_2$ (No. 00-035-0749) are used to index the diffraction peaks. The diffraction peaks of NiO and CoO are too close to differentiate. NiO/CoO refers to a mixture or solid solution of NiO and CoO. Similarly, the diffraction peaks of Ni and Co are also very close, and Ni/Co refers to a mixture or alloy of Ni and Co. (B) The leaching efficiencies of Li, Ni, Co, and Mn from the pristine waste NCM523 and the roasted products in H-cells with an applied voltage of 3.5 V and a solid-to-liquid ratio of 10 g L^{-1} at 90 °C for varying periods of time (6, 12, 24, and 48 h). (C) Kinetics analysis showing the Arrhenius plots for the Co, Mn and Ni leaching from NCM523, the Co leaching from CoO, the Mn leaching from MnO, and the Ni leaching from NiO in 0.05 mol L^{-1} H_2SO_4 solutions. All these oxides were commercially purchased.

The pH gradient was expected to be the driving force for the dissolution of the roasted products (eqn (5)) and the precipitation of transition metal ions (eqn (7)). Therefore, we monitored the change of the pH values in the anode and cathode chambers during water electrolysis at 3.5 V and a solid-to-liquid ratio of 10 g L^{-1} at 90 °C (Fig. S14†). Initially, the anolyte became alkaline (pH = 11.15) due to the presence of water-soluble LiOH in the roasted products (eqn (1)), while the catholyte remained almost neutral. Within only one hour, however, the anolyte turned acidic with the pH value dropping dramatically to 2.28. Meanwhile, the catholyte became basic with pH = 12.18. After 24 hours of electrolysis, the pH values of the anolyte and the catholyte were stable at 1.4–1.6 and 12.2–12.5, respectively. A large and stable pH gradient between the anode and cathode chambers was established. In other words, the electrolysis of water (eqn (4) and (6)), the recombination of H^+ and OH^- at the cross-tube ($H^+ + OH^- = H_2O$), the consumption of H^+ for roasted products leaching (eqn (5)), and the use of OH^- for the precipitation of transition metal ions (eqn (7)) reached a relatively steady state.

Fig. 5B shows the leaching efficiencies of Li, Ni, Co, and Mn from the roasted products and the pristine waste NCM523 powders after electrolysis at 3.5 V for varying periods of time (6, 12, 24, and 48 h) with the same solid-to-liquid ratio 10 g L^{-1} at 90 °C. Remarkably, the leaching efficiencies of Li, Ni, Co and Mn from the roasted products were generally greater. After the 24 h electrolysis of the pristine NCM523, the leaching efficiencies of Li, Ni, Co, and Mn were 95%, 86%, 76% and 27%, respectively. In comparison, the leaching efficiencies of Li, Ni, Co and Mn from the roasted products were 99%, 97%, 82% and 42%, respectively. After the 48 h electrolysis experiment, the leaching efficiencies of Li, Ni, Co and Mn from the roasted products increased to 100%, 99%, 90%, and 72%, respectively.

Fig. S15† shows the XRD patterns for the roasted products and the residues after leaching for various periods of time (6,12, and 24 h) in the anode chamber of the H-cell. The amount of residues after leaching for 48 h was too little to characterize with XRD. The diffraction peaks for NiO and CoO gradually became weaker with time and disappeared after 24 h due to the dissolution. The $LiNi_xCo_yMn_zO_2$ phase was present in all these scans. The γ-MnO_2 and the birnessite-type phase were formed in the residues after 24 hours of leaching; such phases were also observed after the leaching of the pristine waste NCM523 in neutral water electrolysis for 48 hours (Fig. S12A†).

The relatively low leaching efficiency of Mn from the roasted products was attributed to the following factors. First, the acid-soluble MnO was not formed after the reduction roasting at 300 °C for 135 min in 5% H_2. Second, a small amount of NCM phase was still present in the roasted products (Fig. 5A(d)). NCM exhibited a relatively slow leaching kinetics. Nevertheless, the leaching efficiency of Mn would in principle be improved significantly if a pathway could be found to convert all the Mn in NCM523 to the low-valence MnO by H_2 reduction roasting. For example, the roasted product (calcined at 300 °C for 135 min in 5% H_2) could be first subjected to the electrolysis in an H-cell to leach out almost all the Li, Ni, and Co. Afterwards, the residues containing mainly Mn could be collected and subjected to H_2 reduction roasting at a greater temperature (*e.g.*, 850 °C) to produce MnO, similar to the H_2 reduction of the pristine waste $LiMn_2O_4$ as described in Section 3.2.1. Then, the MnO product obtained could be subjected to the electrolysis again in an H-cell to leach out all the Mn ions.

3.3.4. Kinetics analysis for the leaching of transition metals from NCM523. To reveal the leaching kinetics, we explored the leaching behaviors of Co, Mn, and Ni from the commercially purchased NCM523 in 0.05 mol L^{-1} H_2SO_4 for different time lengths (0–50 min) at various temperatures (24–53 °C), as shown in Fig. S16a–S18a.† Based on the curve fitting results, the leaching kinetics of Co, Mn and Ni from NCM523 were all controlled by the surface chemical reactions (Fig. S16c–S18c†), and the activation energies for the leaching of Co, Mn, and Ni from NCM523 were determined to be 42, 42, and 43 kJ mol^{-1}, respectively (Fig. 5C). The values of activation energies were in agreement with the kinetics analysis for the leaching from NCM111 in a previous study.[50] As shown in Fig. 5C, the activation energy for the leaching of Co from NCM523 (42 kJ mol^{-1}) was greater than that from CoO (21 kJ mol^{-1}); in addition, the activation energy for the leaching of Mn from NCM523 (42 kJ mol^{-1}) was also greater than that from pure MnO (16 kJ mol^{-1}). Fig. 5C also shows that the activation energy for the leaching of Ni from NCM523 (43 kJ mol^{-1}) was smaller than that from pure NiO (85 kJ mol^{-1}; see Fig. S19† for the kinetics data and the curve-fitting results). Nevertheless, the leaching efficiency of Ni from NCM523 was smaller than that from the roasted products consisting of CoO/NiO (Fig. 5B). These results suggest that the Ni leaching from the roasted products might be facilitated by the concurrent leaching of Co. More discussion on the kinetics analysis can be found in Note S4.†

3.3.5. Comparison of the amounts of H_2 consumed by reduction and the H_2 produced by electrolysis. The amounts of the H_2 consumed by the reduction roasting and the H_2 produced by a 24 h neutral water electrolysis were compared. A solid-to-liquid ratio of 10 g L^{-1} corresponds to 0.1 g of NCM523 placed in the 10 ml anode chamber of an H-cell. Assuming the ideal chemical reaction between H_2 and NCM (eqn (3)), reducing 0.1 g of NCM523 required merely 0.0005 mol of H_2. In comparison, the amount of H_2 produced by the 24 h electrolysis was calculated to be as high as 0.017 mol supposing a 100% Faraday efficiency. As a result, a scaled-up recycling system may generate a large amount of excessive H_2, which can be stored for other applications such as ammonia synthesis[51] and fuel cells.[52,53]

3.3.6. The precipitation of transition metal ions and the resynthesis of NCM. The amounts of Ni, Co and Mn leached from the roasted product of NCM in the anode chamber were different for different electrolysis experiments (Fig. 5B). These metal ions were transported to the cathode chamber driven by the concentration gradient, electric field and convection. The HER (eqn (6)) on the cathode provided OH^- for the precipitation of the transition metals. It has been reported that Ni^{2+} begins to precipitate at pH = 5.156 and completely precipitates at pH = 8.869, Co^{2+} begins to precipitate at pH = 6.673 and completely precipitates at pH = 9.386, Mn^{2+} begins to precipitate at pH = 7.398 and completely precipitates at pH = 10.151.[54] The mixed hydroxides of the three transition metal ions were obtained in the cathode chamber because the pH value in the cathode chamber was high enough (typically above 12) for complete precipitation. Nevertheless, the proportions of Ni, Co, and Mn in the precipitates were difficult to control, which posed challenges for the subsequent utilization as a precursor for the resynthesis of NCM.

To obtain a high-quality precursor, the universal co-precipitation method reported in a previous study was adopted.[54] In brief, the mixed hydroxides obtained from the electrolysis experiments were first dissolved in dilute H_2SO_4. Additional $NiSO_4$, $CoSO_4$ and $MnSO_4$ were then added to adjust the ratio of Ni : Co : Mn to 5 : 2 : 3. Finally, excessive NaOH solution was added to fully co-precipitate the transition metal ions and produce a high-quality hydroxide precursor with a 5 : 2 : 3 Ni : Co : Mn ratio. Besides, the Li^+ that were leached out were precipitated in the form of Li_2CO_3 following the procedures reported previously.[12] New NCM was resynthesized by calcining the Li_2CO_3 recovered and the hydroxide precursor co-precipitated. In the XRD pattern for the resynthesized powders, the diffraction peaks were well indexed with the hexagonal α-$NaFeO_2$-type structure of the space group $R\bar{3}m$ (Fig. 6a). The obvious splitting of peaks (006)/(012) and (018)/(110) indicated that the degree of cation mixing was small. The XPS spectra confirmed the existence of Ni, Co and Mn in the synthesized powder (Fig. 6b–d). The binding energy of Ni $2p_{3/2}$ was 854.9 eV, consistent with the previous literature on NCM523.[43] The separation of Co $2p_{3/2}$ and Co $2p_{1/2}$ was approximately 15 eV, indicating the valence state of Co as +3.[12] The magnitude of the Mn 3s peak splitting was approximately 4.7 eV, suggesting the

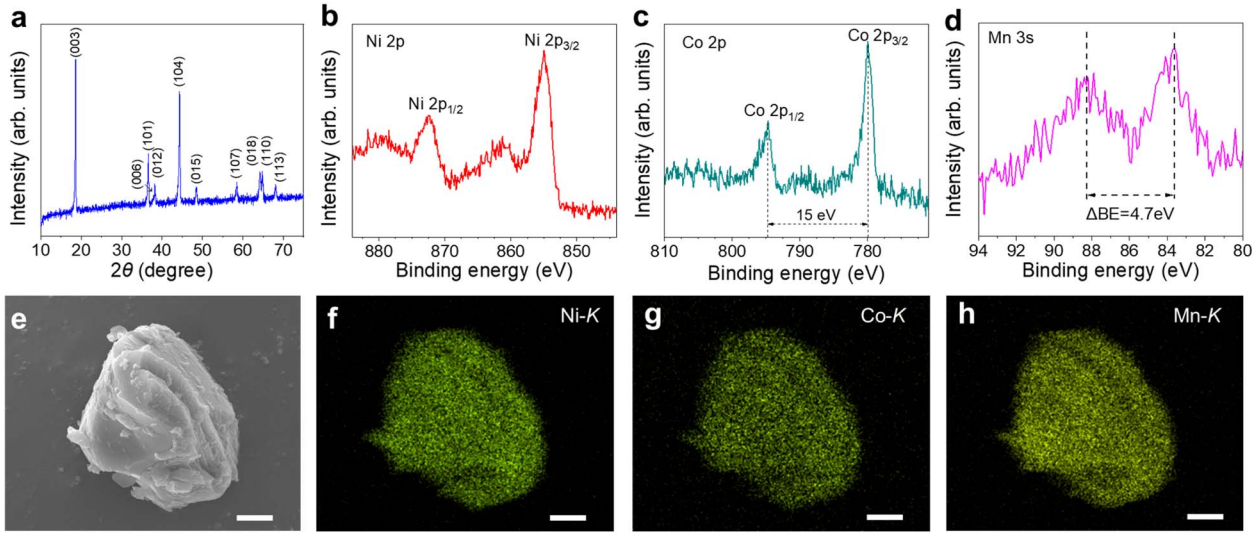

Fig. 6 Characterization of the resynthesized NCM523 powders. (a) XRD pattern, (b) Ni 2p, (c) Co 2p, and (d) Mn 3s XPS spectra. (e) SEM and (f, g, h) EDS mapping of Ni, Co, and Mn of a representative NCM523 particle. Scale bars: 1 μm.

valence state of Mn as +4.[41] The SEM-EDS analysis of the resynthesized powders showed that Ni, Co and Mn were homogeneously distributed throughout the particle (Fig. 6e–h). Detailed evaluation of the electrochemical performance of the regenerated NCM523 as new cathode materials for LIBs is beyond the scope of the current work and will be performed in the future work.

4. Conclusions

In summary, we have demonstrated a sustainable and effective approach that combined H_2 reduction roasting and neutral water electrolysis to recover valuable metals from spent LIBs. H_2 served as a gas reductant to reduce the pristine waste cathode materials to low-valence transition metal oxides that easily dissolved in the subsequent electrolysis. We highlight that the step of the H_2 reduction roasting circumvented a major obstacle to the neutral water electrolysis method (*i.e.*, incompatibility with an external water-soluble reducing agent) and significantly increased the leaching efficiencies of the transition metal ions. For example, the leaching efficiency of Co from the roasted product was almost 4 times greater than that from the pristine waste $LiCoO_2$ in neutral water electrolysers at 3.5 V for 24 h at 60 °C. In a neutral water electrolyser at 3.5 V for 24 h at 90 °C, the leaching efficiency of Mn from the roasted product reached almost 100%, which was approximately 2.5 times greater than that from the pristine waste $LiMn_2O_4$. The H_2 roasting treatment was also effective in improving the leaching efficiencies of Ni, Co, and Mn in the case of recycling NCM523. Besides, the transition metal hydroxides and the Li_2CO_3 recovered were used to resynthesize new NCM523 materials. Moreover, a portion of the H_2 generated by the water electrolysis can be used as the gaseous reducing agent in the first step of roasting, enabling the closed-loop utilization of H_2.

Although the scale up of a chemical process is known to be complex with multiple key factors to be considered,[55] our combined method has great potential for industrial-scale applications. In the first step of H_2 reduction roasting, the relatively mild temperature conditions, compared with those of the current pyrometallurgical methods,[33] suggest a low energy consumption in a scaled-up plant. In addition, lessons and experiences on the scale up could be earned from the fast-developing hydrogen metallurgy industry due to the similarity.[56] Besides, the use of H_2 rather than carbon or carbon monoxide as the reducing agent also cuts down the CO_2 emission and reduces the environmental impact. In the second step of the neutral water electrolysis, the energy consumption can be reduced by optimizing the cell design and the electrocatalytic electrodes to lower the overpotential losses. In the future, the heat required for H_2 reduction roasting and the power for the neutral water electrolysis might be provided by the emerging affordable renewable electricity. Overall, this combined method represents a promising approach for recycling waste cathode materials from spent LIBs in an effective and environmentally friendly manner. It could also be of broad interest and motivate further research on recovering valuable elements from other solid wastes.

Conflicts of interest

There are no conflicts of interest to declare.

Acknowledgements

The authors acknowledge the financial support from ShanghaiTech University. Part of the work was performed at the Analytical Instrumentation Center (Grant No. SPST-AIC10112914) and the Center for High-resolution Electron Microscopy (C*ħ*EM, Grant No. EM02161943) at ShanghaiTech University.

References

1 M. Armand and J. M. Tarascon, *Nature*, 2008, **451**, 652–657.
2 J. B. Goodenough and K. S. Park, *J. Am. Chem. Soc.*, 2013, **135**, 1167–1176.
3 W. Yu, Y. Guo, Z. Shang, Y. Zhang and S. Xu, *eTransportation*, 2022, **11**, 100155.
4 X. Zhang, L. Li, E. Fan, Q. Xue, Y. Bian, F. Wu and R. Chen, *Chem. Soc. Rev.*, 2018, **47**, 7239–7302.
5 M. Jacoby, **https://cen.acs.org/materials/energy-storage/time-serious-recycling-lithium/97/i28**, 2020, accessed October 19, 2020.
6 S. Sun, C. Jin, W. He, G. Li, H. Zhu and J. Huang, *Sci. Total Environ.*, 2021, **776**, 145913.
7 A. Chagnes and B. Pospiech, *J. Chem. Technol. Biotechnol.*, 2013, **88**, 1191–1199.
8 G. Harper, R. Sommerville, E. Kendrick, L. Driscoll, P. Slater, R. Stolkin, A. Walton, P. Christensen, O. Heidrich, S. Lambert, A. Abbott, K. S. Ryder, L. Gaines and P. Anderson, *Nature*, 2019, **575**, 75–86.
9 A. Porvali, A. Chernyaev, S. Shukla and M. Lundström, *Sep. Purif. Technol.*, 2020, 236.
10 P. Liu, L. Xiao, Y. Chen, Y. Tang, J. Wu and H. Chen, *J. Alloys Compd.*, 2019, **783**, 743–752.
11 C. Stinn and A. Allanore, *Nature*, 2022, **602**, 78–83.
12 J. Ni, J. Zhou, J. Bing and X. Guan, *Sep. Purif. Technol.*, 2021, **278**, 119485.
13 J. Zhou, J. Bing, J. Ni, X. Wang and X. Guan, *Mater. Today Sustain.*, 2022, **20**, 100205.
14 L. D. Ellis, A. F. Badel, M. L. Chiang, R. J. Park and Y. M. Chiang, *Proc. Natl. Acad. Sci. U. S. A.*, 2020, **117**, 12584–12591.
15 G. H. Rau, *Environ. Sci. Technol.*, 2008, **42**, 8935–8940.
16 C. Zhou, J. Ni, H. Chen and X. Guan, *Sustain. Energy Fuels*, 2021, **5**, 4355–4367.
17 E. Billy, M. Joulié, R. Laucournet, A. Boulineau, E. De Vito and D. Meyer, *ACS Appl. Mater. Interfaces*, 2018, **10**, 16424–16435.
18 J. Li, G. Wang and Z. Xu, *J. Hazard. Mater.*, 2016, **302**, 97–104.
19 S. Pindar and N. Dhawan, *JOM*, 2019, **71**, 4483–4491.
20 Y. Zhang, W. Wang, Q. Fang and S. Xu, *Waste Manag.*, 2020, **102**, 847–855.
21 J. Xiao, J. Li and Z. Xu, *Environ. Sci. Technol.*, 2017, **51**, 11960–11966.
22 J. Hu, J. Zhang, H. Li, Y. Chen and C. Wang, *J. Power Sources*, 2017, **351**, 192–199.
23 W. Wang, Y. Zhang, X. Liu and S. Xu, *ACS Sustainable Chem. Eng.*, 2019, **7**(14), 12222–12230.
24 Z. Huang, D. Yu, B. Makuza, Q. Tian, X. Guo and K. Zhang, *Front. Chem.*, 2022, **10**, 1019493.
25 J. Xiao, B. Niu and Z. Xu, *J. Hazard. Mater.*, 2021, **418**, 126319.
26 C. Yang, J. Zhang, B. Yu, H. Huang, Y. Chen and C. Wang, *Sep. Purif. Technol.*, 2021, **267**, 118609.
27 Z. Huang, F. Liu, B. Makuza, D. Yu, X. Guo and Q. Tian, *ACS Sustainable Chem. Eng.*, 2022, **10**, 756–765.
28 F. Liu, C. Peng, Q. Ma, J. Wang, S. Zhou, Z. Chen, B. P. Wilson and M. Lundström, *Sep. Purif. Technol.*, 2021, **259**, 118181.
29 J. Zhao, B. Zhang, H. Xie, J. Qu, X. Qu, P. Xing and H. Yin, *Environ. Res.*, 2020, **181**, 108803.
30 O. Levenspiel, Wiley, New York, 1972, p. 367.
31 P. Meshram, B. D. Pandey and T. R. Mankhand, *Chem. Eng. J.*, 2015, **281**, 418–427.
32 W. Gao, J. Song, H. Cao, X. Lin, X. Zhang, X. Zheng, Y. Zhang and Z. Sun, *J. Clean. Prod.*, 2018, **178**, 833–845.
33 B. Makuza, Q. Tian, X. Guo, K. Chattopadhyay and D. Yu, *J. Power Sources*, 2021, **491**, 229622.
34 P. Xu, D. H. S. Tan, H. Gao, S. Rose and Z. Chen, in *Encyclopedia of Energy Storage*, ed. L. F. Cabeza, Elsevier, Oxford, 2022, pp. 98–107.
35 Q. Yang, J. Liu, C. Zhou, J. Ni, E. I. Vovk, Y. Yang, B. Yang and X. Guan, *Mater. Today Chem.*, 2022, **25**, 100949.
36 C. K. Lee and K.-I. Rhee, *Hydrometallurgy*, 2003, **68**, 5–10.
37 L. Li, Y. Bian, X. Zhang, Y. Guan, E. Fan, F. Wu and R. Chen, *Waste Manag.*, 2018, **71**, 362–371.
38 X. Zhu, F. Meng, Q. Zhang, L. Xue, H. Zhu, S. Lan, Q. Liu, J. Zhao, Y. Zhuang, Q. Guo, B. Liu, L. Gu, X. Lu, Y. Ren and H. Xia, *Nat. Sustainability*, 2021, **4**, 392–401.
39 H. Y. Asl and A. Manthiram, *Science*, 2020, **369**, 140–141.
40 P. He, J. Luo, J. He and Y. Xia, *J. Electrochem. Soc.*, 2009, **156**, A209.
41 M. Toupin, T. Brousse and D. Bélanger, *Chem. Mater.*, 2002, **14**, 3946–3952.
42 S. Chang, Y. Chen, Y. Li, J. Guo, Q. Su, J. Zhu, G. Cao and W. Li, *J. Alloys Compd.*, 2019, **781**, 496–503.
43 Z. Fu, J. Hu, W. Hu, S. Yang and Y. Luo, *Appl. Surf. Sci.*, 2018, **441**, 1048–1056.
44 N. Nitta, F. Wu, J. T. Lee and G. Yushin, *Mater. Today*, 2015, **18**, 252–264.
45 K. M. Shaju and P. G. Bruce, *Adv. Mater.*, 2006, **18**, 2330–2334.
46 D. Wu, X. Liu, P. Gao, L. He and J. Li, *Ceram. Int.*, 2022, **48**, 11228–11237.
47 X. Wang, X. Zhang, Y. Sun, H. Zhang, C. Pei, M. Zhao, J. Zhou, Q. Tang, H. Chen, B. Xi, Y. Qi, Z. Liu, G. Li and X. Guan, *Appl. Surf. Sci.*, 2023, **624**, 157103.
48 M. Li and J. Lu, *Science*, 2020, **367**, 979–980.
49 H. Darjazi, S. J. Rezvani, S. Brutti and F. Nobili, *Electrochim. Acta*, 2022, **404**, 139577.
50 X. Zhang, H. Cao, Y. Xie, P. Ning, H. An, H. You and F. Nawaz, *Sep. Purif. Technol.*, 2015, **150**, 186–195.
51 Z. Tang, X. Meng, Y. Shi and X. Guan, *ChemSusChem*, 2021, **14**, 4697–4707.
52 X. Guan, J. Jiang, J. Lattimer, M. Tsuchiya, C. M. Friend and S. Ramanathan, *Energy Technol.*, 2016, **5**, 616–622.
53 Y. Zhou, X. Guan, H. Zhou, K. Ramadoss, S. Adam, H. Liu, S. Lee, J. Shi, M. Tsuchiya, D. D. Fong and S. Ramanathan, *Nature*, 2016, **534**, 231–234.
54 H. Zou, E. Gratz, D. Apelian and Y. Wang, *Green Chem.*, 2013, **15**, 1183–1191.
55 J. R. Hitchin, *Nat. Rev. Methods Primers*, 2022, **2**, 28.
56 J. Tang, M.-s. Chu, F. Li, C. Feng, Z.-g. Liu and Y.-s. Zhou, *Int. J. Miner. Metall. Mater.*, 2020, **27**, 713–723.